Redox Biology 45 (2021) 102026

Contents lists available at ScienceDirect

Redox Biology

journal homepage: www.elsevier.com/locate/redox

Increased glycolysis is an early consequence of palmitate lipotoxicity mediated by redox signaling

Pamela A. Kakimoto [a,*], Julian David C. Serna [a], Vitor de Miranda Ramos [a], Antonio Zorzano [b], Alicia J. Kowaltowski [a,**]

[a] Departamento de Bioquímica, Instituto de Química, Universidade de São Paulo, São Paulo, Brazil
[b] Institute for Research in Biomedicine (IRB Barcelona), Departament de Bioquímica I Biomedicina Molecular, Facultat de Biologia, Universitat de Barcelona, CIBER de Diabetes y Enfermedades Metabólicas Asociadas (CIBERDEM), Instituto de Salud Carlos III, Barcelona, Spain

ARTICLE INFO

Keywords:
Palmitic acid
Mitochondria
Glycolysis
Oxidative stress
Reactive oxygen species

ABSTRACT

Exposure to toxic levels of fatty acids (lipotoxicity) leads to cell damage and death and is involved in the pathogenesis of the metabolic syndrome. Since the metabolic consequences of lipotoxicity are still poorly understood, we studied the bioenergetic effects of the saturated fatty acid palmitate, quantifying changes in mitochondrial morphology, real-time oxygen consumption, ATP production sources, and extracellular acidification in hepatoma cells. Surprisingly, glycolysis was enhanced by the presence of palmitate as soon as 1 h after stimulus, while oxygen consumption and oxidative phosphorylation were unchanged, despite overt mitochondrial fragmentation. Palmitate only induced mitochondrial fragmentation if glucose and glutamine were available, while glycolytic enhancement did not require glutamine, showing it is independent of mitochondrial morphological changes. Redox state was altered by palmitate, as indicated by NAD(P)H quantification. Furthermore, the mitochondrial antioxidant mitoquinone, or a selective inhibitor of complex I electron leakage (S1QEL) further enhanced palmitate-induced glycolysis. Our results demonstrate that palmitate overload and lipotoxicity involves an unexpected and early increase in glycolytic flux, while, surprisingly, no changes in oxidative phosphorylation are observed. Interestingly, enhanced glycolysis involves signaling by mitochondrially-generated oxidants, uncovering a novel regulatory mechanism for this pathway.

1. Introduction

High concentrations of nonesterified fatty acids in the plasma are a common feature in the metabolic syndrome, and reflect the inability to suppress lipolysis through insulin signaling, or inadequate capacity to store energetic surpluses [1–3]. Palmitic acid, a sixteen carbon saturated fatty acid, is the most abundant saturated fatty acid in human blood [3–5]. In excess, palmitate causes lipotoxicity, a disturbance promoted by lipid overload and/or lipid accumulation that compromises function. Palmitate overload can trigger lipid accumulation, insulin resistance, endoplasmic reticulum stress and oxidative imbalance, often culminating in cell death [6–8]. Piccolis et al. [9] demonstrated that the most upregulated stress responses after 24 h of palmitate overload are apoptosis, autophagy, and endoplasmic reticulum stress [9]. The accumulation of glycerolipids, mainly in the di-saturated form, is probably the trigger for this toxicity [10,11], but the metabolic pathways sustaining these changes induced by palmitate have not been elucidated.

Mitochondrial function is often a suggested target for lipotoxicity, since these organelles are central in metabolic control and lipid homeostasis, in addition to being involved in cell death mechanisms. Mitochondria are dynamic and can quickly adapt to their surroundings with profound changes in function and form [12,13]. In addition to their roles related to ATP production and cell death, they act as hubs regulating calcium signaling, supplying intermediates for lipid synthesis, and modulating the production and removal of oxidants such as superoxide radical anions. Concomitantly, mitochondria sense nutrient availability and cooperate with metabolism-regulating pathways, including responses to insulin and its downstream effectors [14–18].

Mitochondrial flexibility not only involves their functional plasticity, but also their physical size and shape: nutrient oversupply predominantly promotes mitochondrial fragmentation, while nutrient starvation is mostly associated with elongation and a more continuous network

* Corresponding author. Av. Prof. Lineu Prestes, 748, Cidade Universitária, 05508-000, São Paulo, SP, Brazil.
** Corresponding author. Av. Prof. Lineu Prestes, 748, Cidade Universitária, 05508-000, São Paulo, SP, Brazil.
E-mail addresses: pamela.kakimoto@gmail.com (P.A. Kakimoto), alicia@iq.usp.br (A.J. Kowaltowski).

https://doi.org/10.1016/j.redox.2021.102026
Received 4 April 2021; Received in revised form 14 May 2021; Accepted 24 May 2021
Available online 1 June 2021

[16,17,19]. Shorter and more rounded mitochondria are usually thought to be less efficient at producing ATP than elongated ones [20]. An increased supply of fatty acids can change the morphology of the mitochondrial network, and saturated fatty acid overload has been shown to promote mitochondrial fragmentation [21–23] or fusion [22,24], depending on acyl chain length and if unsaturated fatty acids are also present. The functional consequences for lipotoxicity of these changes in mitochondrial morphology still remain to be understood.

While most studies evaluated cellular features at later timepoints of palmitate overload (>12 h), here we describe the early mitochondrial morphological and bioenergetic outcomes of lipotoxicity, to uncover its trigger mechanisms. Using real time measurements, we identified that mitochondrial oxygen consumption is not disturbed by palmitate overload for the first 6 h, despite overt mitochondrial fragmentation and cellular reductive imbalance. Interestingly, palmitate largely upregulated ATP synthesis through glycolysis early on. We demonstrate that the production of mitochondrial oxidants is associated with this unexpected metabolic rewiring promoted by palmitate, uncovering new mechanisms involved in the regulation of glycolytic rates.

2. Results

2.1. Palmitate promotes mitochondrial fragmentation and triglyceride accumulation

Palmitate overload is known to promote mitochondrial fragmentation in many cell types [21–23], but the relationship between these morphological changes and functional bioenergetic consequences has not been established. We observed that exposure to 0.2 mM palmitate for 6 h resulted in overt mitochondrial fragmentation in human hepatoma PLC/PRF/5 cells (Fig. 1A shows typical images quantified in Fig. 1C, where the main mitochondrial phenotype per cell - short, intermediate, or long - was registered in the presence or absence of palmitate). A prolonged palmitate stimulus of 24 h further increased the

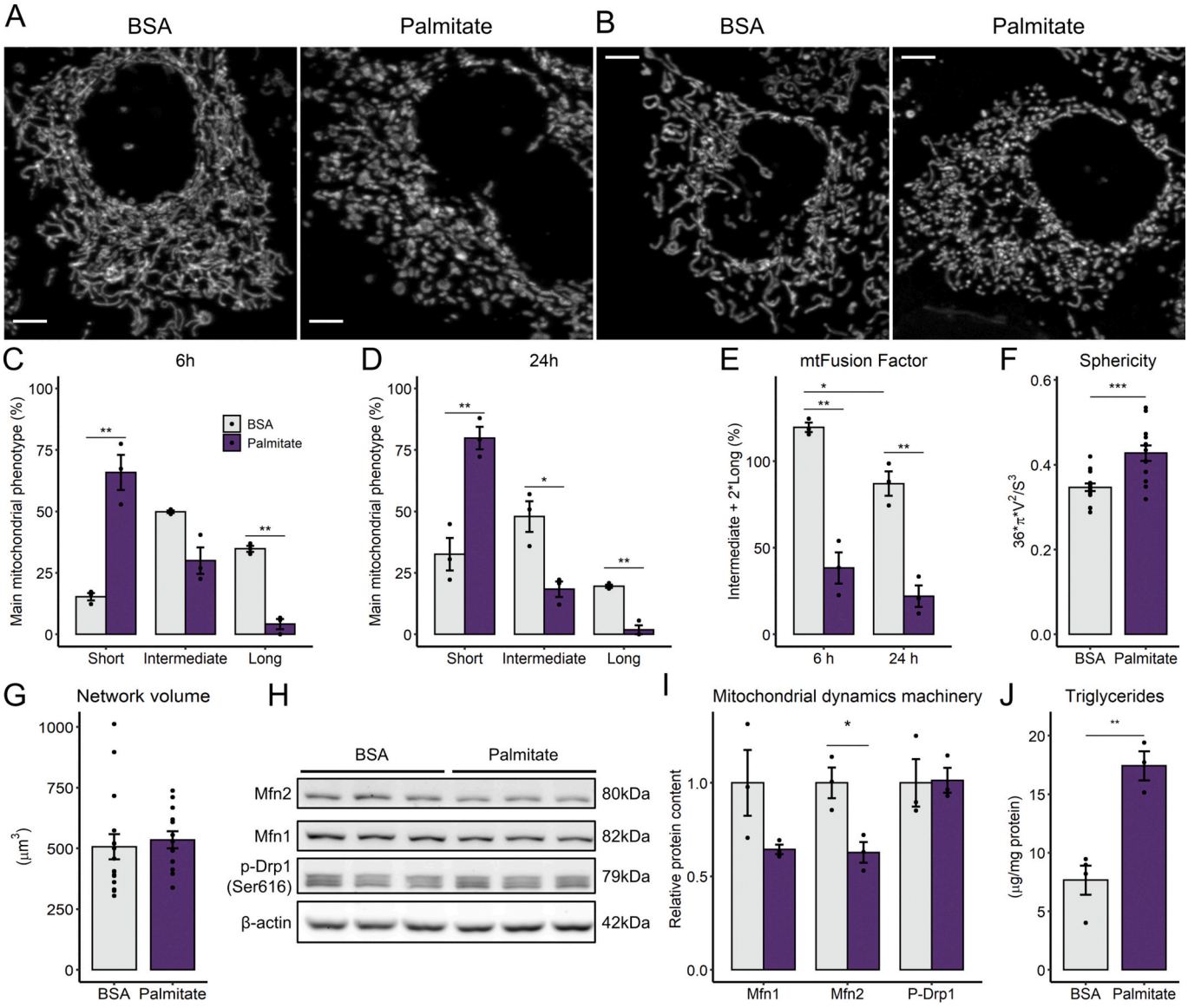

Fig. 1. Palmitate overload promotes mitochondrial fragmentation and triglyceride accumulation - Cells were incubated with palmitate/BSA (0.2 mM/0.25%) for 6 or 24 h. Live mitochondrial morphology was evaluated by confocal microscopy in cells loaded with 0.4 µM TMRM at 6 h (A and C) or 24 h (b and D). Morphological parameters were measured as described in the Methods section, in cell populations (C–E) or individual cells (F–G). Lysates were obtained and blots performed (panels H and I). Triglycerides were extracted and quantified after 6 h of palmitate incubation (J). * = $p < 0.05$, ** = $p < 0.01$, *** = $p < 0.001$ *t*-test (Panels C, D, F, G,I, J) or two-way ANOVA followed by Tukey's post-test (E). Data are means +/- SD. Filled circles represent independent experiments. In F-G, filled circles represent individual cells obtained from 3 independent experiments. Scale bar = 5 µm.

fraction of short mitochondria (Fig. 1B and D). These morphological changes were confirmed by the decrease in mitochondrial fusion factor (Fig. 1E), a measurement of elongated mitochondrial morphology, and by the automated quantification of the mitochondrial population, in which individual organelle sphericity (Fig. 1F), a measure of mitochondrial fragmentation, is increased. Importantly, no changes were detected in total mitochondrial network volume (Fig. 1G).

Next, we measured the levels of proteins responsible for mitochondrial morphological homeostasis. Protein levels of mitofusin-2 were decreased by palmitate after 6 h, while the mitofusin-1 trended toward a decrease, and Ser616-phosphorylated Drp-1 (a fission protein) was unchanged (Fig. 1H–I), suggesting that shorted mitochondria were a consequence of a diminished mitochondrial fusion, not increased fission. In parallel, we observed that palmitate treatment induced significant triglyceride accumulation at 6 h (Fig. 1J) and lipid droplet formation at 24 h (Fig S1). These results confirm the ability of palmitate overload to replicate mitochondrial fragmentation and lipid accumulation in our cells, validating this lipotoxicity model, with strong results on mitochondrial morphology detected as early as 6 h of incubation.

2.2. *Palmitate upregulates glycolysis without disturbing mitochondrial oxygen consumption*

Due to the overt changes in mitochondrial morphology induced by palmitate lipotoxicity, we expected to find changes in mitochondrial function, and particularly in oxidative phosphorylation supported by different substrates. Indeed, changes in the predominant shape of the mitochondrial network in response to their microenvironment have been associated with modifications in bioenergetic function [13,20]. To study maximized oxidative phosphorylation (known as state 3 respiration) in the presence of specific substrates, cell plasma membranes were permeabilized in order to promote oxidative phosphorylation by adding excess ADP, while preserving cell and mitochondrial architecture [25,26]. Under these conditions, we found no differences in respiration in cells that had undergone 6 h of palmitate lipotoxicity using a combination of respiratory substrates (labelled as "all" in Fig. 2A), pyruvate plus malate, glutamate plus malate, or succinate plus the complex I inhibitor rotenone. This indicates that maximum oxidative phosphorylation capacity is unchanged despite overt morphological changes promoted by lipotoxicity. Oxygen consumption rates (OCRs) were also measured by inhibiting ATP-synthase with oligomycin (state 4 respiration), a condition used to assess inner membrane impermeability to protons or their re-entry through other transporters/enzymes such as the adenine nucleotide translocator, nicotinamide nucleotide transhydrogenase or the phosphate carrier, as well as electron leakage due to the production of superoxide radicals. Under these conditions, respiratory rates were not significantly changed by palmitate, although rates supported by succinate in the presence of rotenone tended toward an increase (Fig. 2B). Despite no significant changes in respiratory states, palmitate decreased overall respiratory control ratios (state 3/state 4) (Fig. 2C), i.e., respiration is globally less coupled to ATP synthesis.

While permeabilized cell respiratory measurements uncover maximal oxidative phosphorylation capacity, they do not assess physiological ATP production rates nor account for possible impacts of changes in cytosolic metabolic pathways. To determine how palmitate lipotoxicity affected cellular metabolism, we followed real-time oxygen consumption rates in intact cells just after palmitate treatment, up to 6 h (Fig. 3A). Consistently with permeabilized cell measurements, oxygen consumption rates of palmitate-treated cells were not significantly affected over time compared to the BSA controls (Fig. 3A). However, and quite surprisingly, palmitate promoted a highly significant increase in extracellular acidification rates (ECARs; Fig. 3B), which were measured in parallel by extracellular flux analysis. ECARs reflect extracellular acidification rates, and not the pH itself, and are thus not influenced by the acute addition of different substrates, such as palmitate. Indeed, control experiments determined the effect of the addition of BSA and palmitate to media in the absence of cells, and the small changes observed were subtracted as background quantifications to establish ECARs, a reflection of cellular acidification effects.

Differences in ECARs promoted by palmitate under our conditions may be related to lactate production, changes in tricarboxylic acid cycle flux (due to CO_2 production), ATP turnover, or other acid-generating catabolic processes [27]. To evaluate the acidification source under our conditions, we measured lactate secreted into the supernatant and monitored ECARs in the presence of 2-deoxyglucose, an inhibitor of hexokinases, the first enzymes in the glycolytic pathway. In palmitate-treated cells, accumulated lactate is significantly increased over time (Fig. 3C). Furthermore, 2-deoxyglucose blunted the ECAR increase (Fig. 3D–E) without changing OCRs, indicating this effect was not related to a lack of substrate availability to mitochondria (Fig. 3F).

Importantly, palmitate treatment very strongly enhanced the contribution of glycolysis toward ATP production (Fig. 3G), which can be quantified by extracellular flux analysis, as described in the Methods section. Interestingly however, total ATP production is equal (Fig. 3H). Intriguingly, we found that the cells were not oxidizing palmitate, since etomoxir, a CPT1 inhibitor which avoids the entry of fatty acids into mitochondria, had no significant effect on OCR or ECAR (Fig S2). Furthermore, atglistatin, a selective inhibitor of adipose triglyceride lipase (the major regulator of triglyceride turnover in liver [28]), had no effect on palmitate-stimulated ECAR or glycolysis (Fig S3),

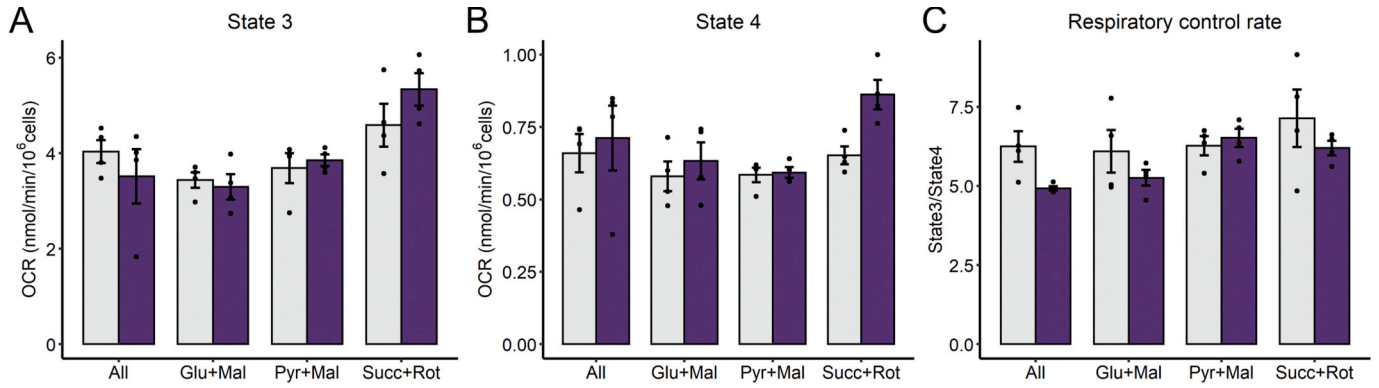

Fig. 2. Early palmitate exposure preserves overall mitochondrial respiration. After 6 h of palmitate incubation, cells were tripsinized and resuspended in respiratory buffer and the substrates indicated, as described in the Methods section. Cells were permeabilized and oxygen consumption rates were monitored with the sequential addition of ADP (1 mM, state 3 respiration, A) and oligomycin (1.3 μM, state 4 respiration, B). Respiratory control ratios were calculated as state3/state4 (Panel C). Two-way ANOVA followed by Tukey's post-test. Palmitate effect is only significant in RCR (C, $p = 0.044$). Bar plots are means +/- SD. Filled circles represent independent experiments.

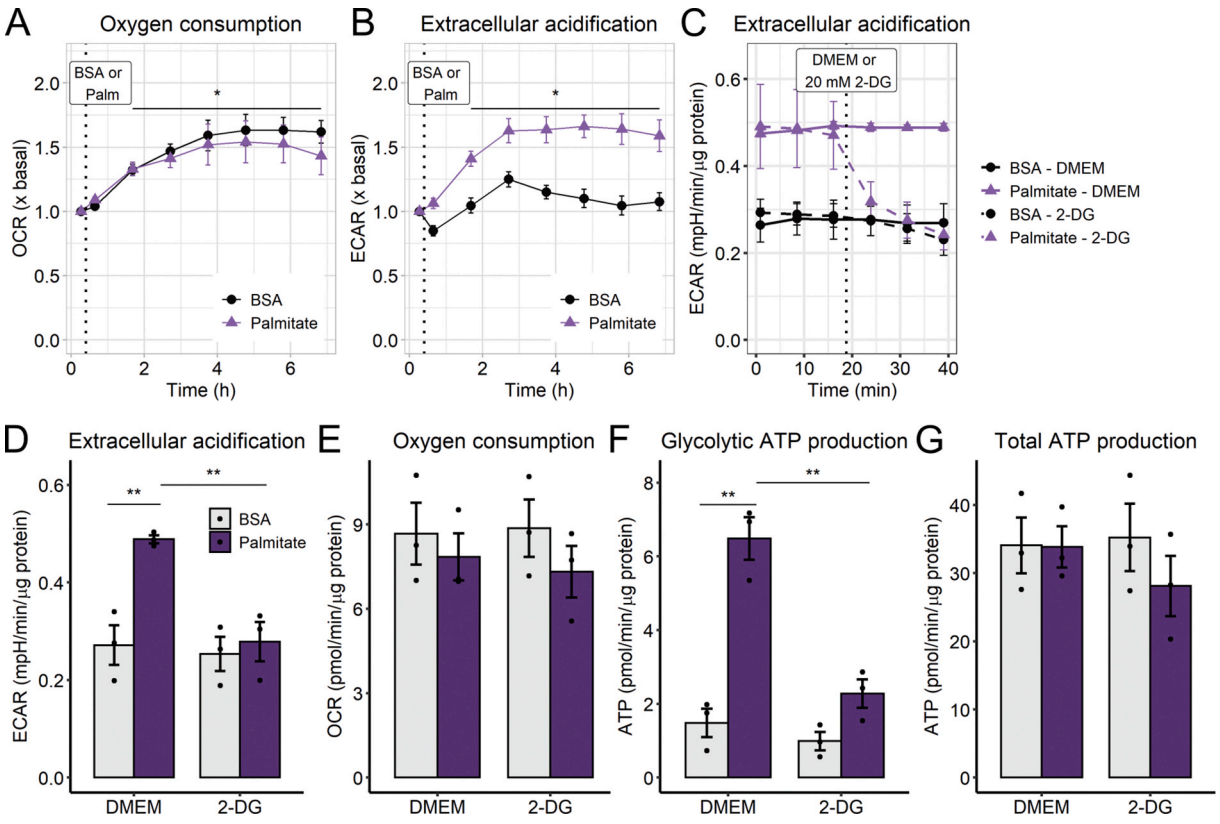

Fig. 3. Palmitate overload increases glycolytic flux - Real-time OCRs and ECARs were measured in a Seahorse XFe24 analyzer over 6 h after 0.2 mM palmitate injection, indicated by the dotted line (A–B). ECARs and OCRs were measured after 6 h palmitate incubation and modulated by 2-deoxyglucose (C–E). Glycolytic ATP and total ATP production were calculated as described in the Methods section (F–G). In A and B, * = $p < 0.05$ for time effect, two-way ANOVA repeated measurements. In D-G, ** = $p < 0.01$ two-way ANOVA followed by Tukey's post-test. OCR and ECAR plots are means +/- SEM. Bar plots are means +/- SD. Filled circles represent independent experiments.

demonstrating that the metabolic shift is not related to changes in lipolysis nor lipophagy [29]. From these results, we conclude that increased mitochondrial fragmentation occurs independently of changes in mitochondrial oxygen consumption and ATP production after palmitate exposure. Surprisingly, our results show that glycolytic flux is increased as soon as 1 h of palmitate treatment, meaning this metabolic switch is the most significant early metabolic outcome of palmitate-induced lipotoxicity.

2.3. Mitochondrial fragmentation and glycolytic rates are independently modulated by substrate availability

Since it was quite surprising that a fatty acid could induce a significant increase in glycolytic ATP production, we found it important to further characterize this effect, by examining the role of different substrates present in culture media toward the metabolic shift. Cells were treated with palmitate when glucose and/or glutamine-deprived for 6 h. Mitochondrial fragmentation was promoted only in full media, i.e., DMEM containing both glucose (Glc) and glutamine (Gln) (Fig. 4A–B). There was a significant decrease in mitochondrial OCRs with glutamine deprivation (Fig. 4C), demonstrating the important role of this amino acid, which feeds into the TCA cycle and sustains mitochondrial ATP production even when glucose is absent (Gln group). The presence of palmitate did not change total ATP production in any group, but glutamine deprivation (no additions and Glc groups) reduced it significantly (Fig. 4E).

Interestingly, mitochondrial fragmentation was not necessary for the activation of ATP synthesis from glycolysis, as this occurred both in the combined presence of glucose and glutamine, and with glucose alone (Fig. 4F). From these results, we can conclude that the cells have high flexibility in nutrient use, and that palmitate does not hamper ATP production, but instead promotes a shift towards glycolysis only if glucose is available (Fig. 4G). We note that dependency of glycolysis on the presence of exogenous glucose is not an obvious given, since hepatic cells have preserved glycogen synthesis and degradation machinery [30]. Our results also suggest that carbon intermediates other than glucose do not play a significantly role in lactate production in this system.

2.4. Redox imbalance in palmitate-induced metabolic plasticity

Lipid overload is often associated with mitochondrially-generated oxidative imbalance [31,32]. To assess cellular redox state, we measured the NAD(P)H pool, since NADPH, which can be produced from mitochondrial NADH or cytosolic glucose [33], and is essential to maintain reduced glutathione and thioredoxin, which participate in the main hydrogen peroxide-removing systems [34]. NAD(P)H was quantified in cells by autofluorescence (Fig S4). Surprisingly, we observed that palmitate treatment promotes a large increase in the total NAD(P) pool (Fig. 5A), while NAD(P)H/$NADP^+$ ratios are markedly lower in palmitate versus control cells (Fig. 5B). These results indicate that palmitate leads to redox changes. However, this assay cannot separate different cellular compartments, as mitochondrial modulation will also change NAD(P)H redox state in the cytosol, since the pools are connected by the reversible malate-aspartate shuttle in hepatic cells [35].

To investigate the production of oxidants by the mitochondrial electron transport chain, we again used permeabilized cells, in an approach similar to Fig. 2, but measuring H_2O_2 released from mitochondria. As expected, state 4 respiration (in the absence of oxidative phosphorylation) exacerbated H_2O_2 release in comparison to state 3,

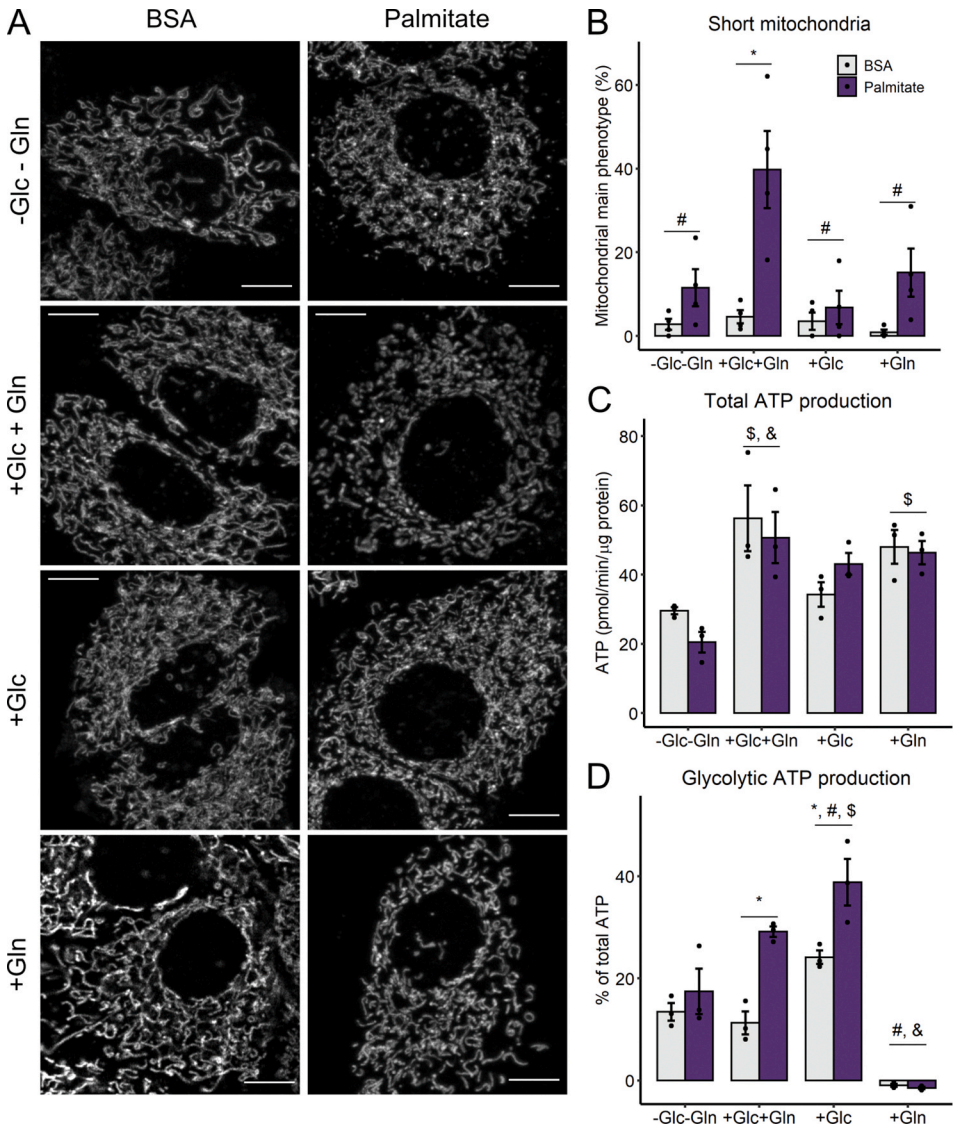

Fig. 4. Palmitate-induced metabolic shift requires glucose, but not mitochondrial network fragmentation - Cells were incubated with palmitate/BSA (0.2 mM/0.25%) for 6 h in media without glucose nor glutamine (-Glc-Gln), or in the presence of glucose and glutamine (Glc + Gln), only glucose (Glc), or only glutamine (Gln). Live mitochondrial morphology was evaluated by confocal microscopy at 6 h after 50 nM Mitotracker Deep Red loading (A). Mitochondrial network morphology was classified as described in the Methods section (B). ATP production was calculated as described in the Methods section (C–D). * = $p < 0.05$ or ** = $p < 0.01$; $ $p < 0.05$ vs. –Glc-Gln; # = $p < 0.05$ vs. Glc + Gln. Two-way ANOVA followed by Tukey's post-test. Bar plots are means +/- SD. Filled circles represent independent experiments. Scale bar = 10 µm. (For interpretation of the references to color in this figure legend, the reader is referred to the Web version of this article.)

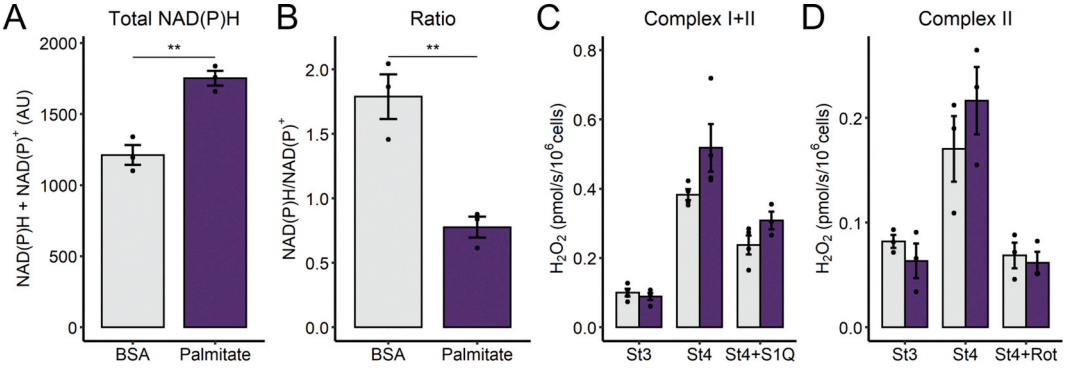

Fig. 5. Palmitate affects redox balance. After 6 h of palmitate incubation, cells were tripsinized and resuspended in DMEM (A and B) or respiratory buffer and the substrates indicated (C and D), as described in the Methods section. NAD(P)H content was assessed in intact cells resuspended in DMEM media containing palmitate or BSA in the fluorimeter. Cells were challenged with rotenone (1 µM) plus antimycin A (1 µM), to promote maximal reduction (A and B). Hydrogen peroxide production was monitored in permeabilized cells by Amplex Red oxidation upon the sequential addition of ADP (1 mM, state 3), oligomycin (1.3 µM), and S1QEL (10 µM) or rotenone (1 µM). In A and B, ** = $p < 0.01$, Student's t-test. In C and D, Two-way ANOVA followed by Tukey's post-test are described in the text. Bar plots are means +/- SD. Filled circles represent independent experiments. (For interpretation of the references to color in this figure legend, the reader is referred to the Web version of this article.)

both with mitochondria energized by complex I and II substrates (Fig. 5C and D). Palmitate-treated cells (dark columns) showed a trend toward an increase in H_2O_2 release with all substrates (2-way ANOVA, FA*Inhibitor interaction, $p = 0.06$). Interestingly, S1QEL1.1, an inhibitor of superoxide/hydrogen peroxide production at complex I site Q, significantly decreased this generation, suggesting a relevant participation of this site. Similarly, succinate-induced reverse transport was suppressed by rotenone.

2.5. Oxidative imbalance promotes glycolysis

Based on the results seen up to now, we hypothesized that redox signals could play a decisive role in the upregulation of glycolytic ATP synthesis promoted by palmitate. We thus evaluated directly if changing redox balance could regulate glycolysis. To do so, we used the naphthoquinone analogue menadione, which increases superoxide formation and lowers NADPH levels [36]. Not unexpectedly, menadione treatment resulted in increased OCRs as a consequence of enhanced proton leak and non-mitochondrial oxygen consumption (Fig 6A, D-E), thus affecting mitochondrial integrity, a result which differs from the effects of palmitate seen previously. Menadione also enhanced ECARs (Fig. 6B), without changing total ATP production (Fig. 6F). Interestingly, the contribution of glycolysis toward ATP production (Fig. 6G) was almost 3-fold higher with menadione than in the DMSO control, suggesting once again that 6 h of redox imbalance is sufficient to remodel cellular metabolism through glycolytic activation, without compromising net ATP production, irrespective of changes in OCRs.

To evaluate the contribution of mitochondrially-generated oxidants toward palmitate-induced glycolysis, we pre-treated the cells with the mitochondrial antioxidant Mitoquinone (MitoQ) for 20 min and added palmitate, while following OCRs and ECARs for up to 2 h. MitoQ is targeted specifically to respiring mitochondria, and cycles through reduced and oxidized forms in the inner membrane, acting as a scavenger of leaked electrons. It cannot be oxidized by complex III, but is recycled by complex II [37]. We found that MitoQ increased glycolytic ATP production, while also inhibiting mitochondrial oxygen consumption and increasing the proton leak, in a concentration-dependent manner (Fig. 7A–F). Thus, the effects of MitoQ on ATP sources are not straightforward, as it suppresses mitochondrial respiration and significantly reduces total ATP production even when used at submicromolar concentrations (Fig. 7A and E), a potential side-effect of this often-used antioxidant, which may be underrecognized in the literature. Despite the potential interference of changes in respiration, the glycolytic shift promoted by palmitate was higher in the presence of 0.5 μM MitoQ (Fig. 7G), suggesting an interaction between the two redox stimuli, while 1 μM MitoQ was found to be overtly toxic for mitochondrial function.

In order to use a more specific antioxidant approach and avoid mitochondrial toxicity, we tested the effects of S1QEL1.1 and S3QEL2 (suppressors of complex I and III site Q electron leaks, respectively), small molecules which were found to block superoxide production from the electron transport chain without compromising electron flow to complex IV-bound oxygen [38,39]. Despite prior reports that these molecules do not hamper respiration, we observed that S3QEL, but not S1QEL (both at 10 μM), lowered oxygen consumption rates (Fig 8A, C), but did not affect total ATP production (Fig. 8D) in our cells. No significant effects were seen on ECARs (Fig. 8B). Interestingly, both modulators exacerbated glycolysis in palmitate-treated cells, and S3QEL also

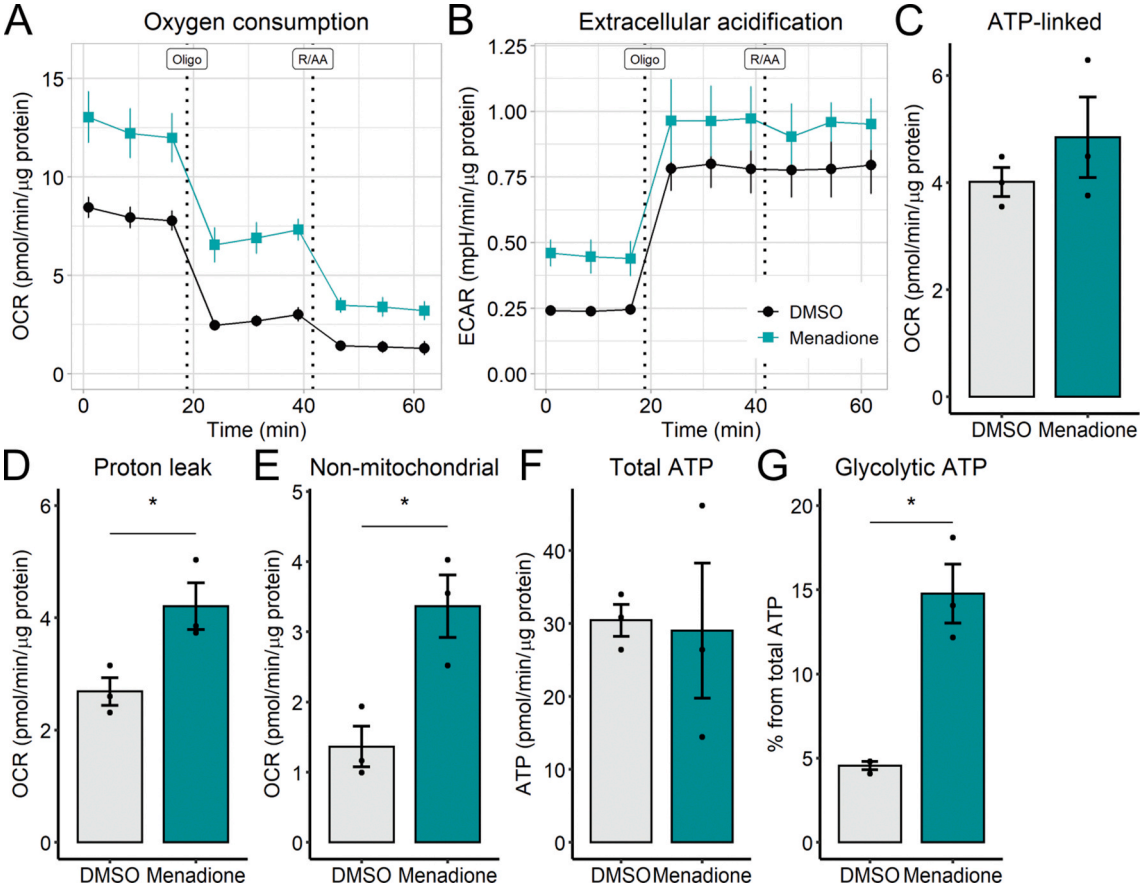

Fig. 6. Menadione increases glycolytic flux - Cells were incubated with 10 μM menadione for 6 h. Vehicle is 0.1% DMSO. Real-time OCRs and ECARs were measured in a Seahorse XFe24 analyzer after 6 h. ATP production was calculated as described in the Methods section. * = $p < 0.05$ Student's *t*-test. OCR and ECAR plots are mean +/- SEM. Bar plots are means +/- SD. Filled circles represent independent experiments.

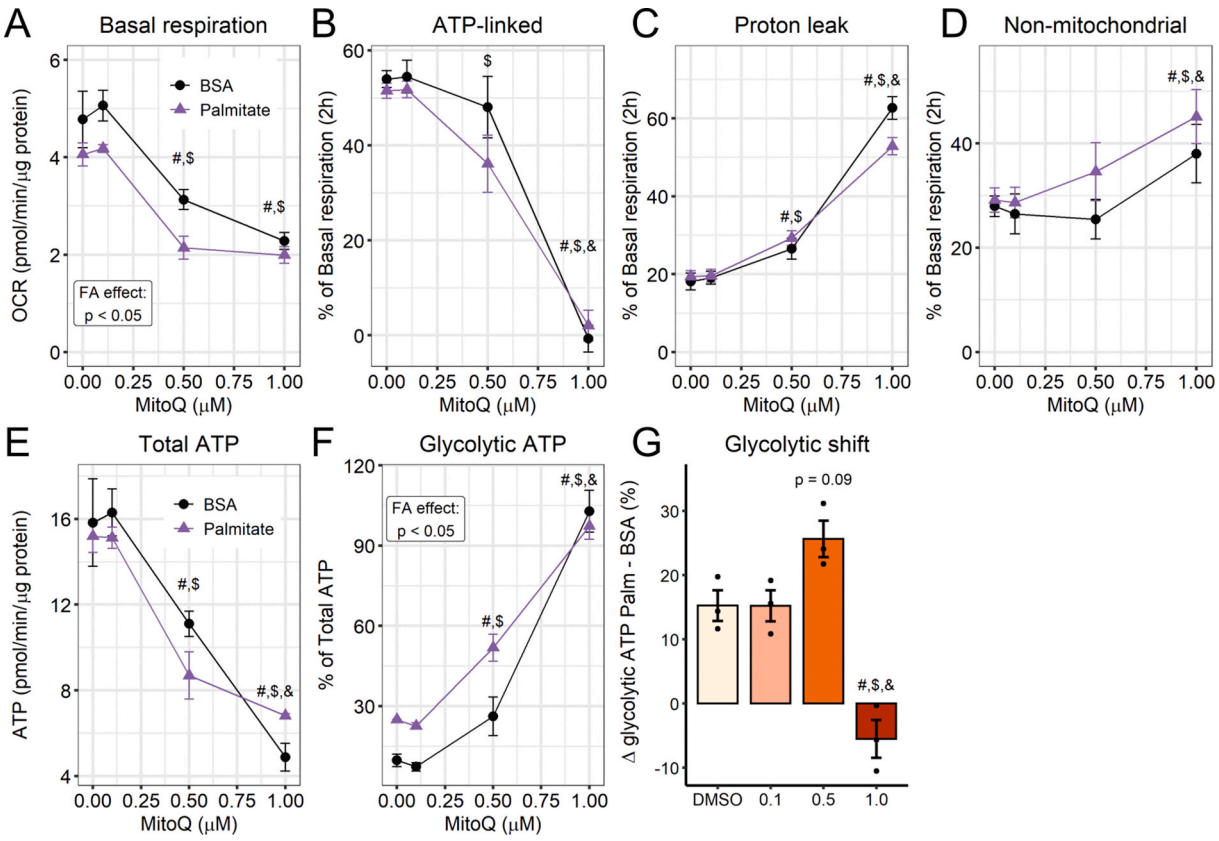

Fig. 7. Mitoquinone increases glycolytic flux - Cells were incubated with 0.1–1.0 µM mitoquinone followed by 2 h of palmitate/BSA (0.2 mM/0.25%). Vehicle is 0.1% DMSO. Real-time OCRs and ECARs were measured in a Seahorse XFe24 analyzer. ATP production was calculated as described in the Methods section. Glycolytic shift was calculated as the difference between palmitate and BSA glycolytic ATP production (from data shown in figure F). # = $p < 0.05$ vs DMSO, $ = vs 0.1, & = vs 0.5. In A-F, Two-way ANOVA. In G, one-way ANOVA. Line plots are mean +/- SEM. Bar plots are means +/- SD. Filled circles represent independent experiments. (n = 3).

increased glycolytic flux in BSA controls (Fig. 8E). These results suggest that both I_Q and III_Q oxidant production sites provide signals that control cytoplasmic ATP production. I_Q effects are disassociated from mitochondrial respiratory inhibition and are therefore specifically attributable to redox signaling. Overall, these results demonstrate that palmitate and redox state are important determinants of glycolytic flux, uncovering new mechanisms regulating glycolysis and involved in lipotoxicity.

3. Discussion

Palmitate overload is well known to promote lipotoxicity in many cell types [21,22], but while the cell biology of lipotoxicity has been extensively explored, the metabolic effects of palmitate that trigger these cellular responses are still unclear. Here, we studied the early metabolic effects of palmitate overload, and how these were related to mitochondrial morphology and function. We have previously found that neither palmitate nor oleate overload for 24 h promote changes in mitochondrial oxygen consumption in BV2 microglial cells, which is surprising, since palmitate is known to promote overt mitochondrial network fragmentation under these conditions [21,22,40]. Additionally, significantly decreased glycolysis and distinct lipidic species accumulation was observed in this inflammatory cell line [40].

Prior studies in hepatic cells [41–43] suggested that palmitate promoted a late decrease in inner mitochondrial membrane potentials and increased oxygen consumption, secondary to calcium efflux from the ER and increased glutamine catabolism [44]. This is compatible with results showing that longer palmitate exposure times are associated with mitophagy inhibition in primary hepatocytes and HepG2 cells (Yu et al., 2019, [45]; lower mitochondrial turnover could result in a less coupled mitochondrial population. We should note, however, that while mitochondrial function in intact cells is reliably evaluated by oxygen consumption rates [46], uncalibrated mitochondrial inner membrane potential estimates are much more artifact-prone [47], particularly when overt changes in morphology occur [26,48]. Furthermore, these late changes in energy metabolism may be a consequence of imbalances promoted by lipotoxicity, and not the initial causes.

Surprisingly, our experiments here show that, within 1 h of incubation, palmitate strongly increases glycolytic flux. An associated increase in glycolytic ATP production occurred, as soundly confirmed by flux quantifications and 2-deoxyglucose-promoted inhibition of extracellular acidification. This occurred without disturbing mitochondrial oxygen consumption (Fig. 3) nor modulating mitochondrial respiratory states (Fig. 2) for up to 6 h in intact cells, demonstrating that the effect is related to glycolytic regulation, and not lack of mitochondrial substrates, organellar damage or changes in mitophagy and mitochondrial mass. In fact, added palmitate was not oxidized, since etomoxir, a CPT1 inhibitor which prevents uptake of the fatty acid into mitochondria [49], had no effects on OCRs or ECARs (Fig S1). Cytosolic palmitate has previously been found to rewire the citric acid cycle and promote modified use of carbon sources [50], which is compatible with our results showing metabolic plasticity promoted by this fatty acid in the cytosol.

After 6 h under the same conditions of palmitate treatment, mitochondria were predominantly fragmented (Fig. 1 A and B). However, substrate availability studies show that fragmentation and the increase in glycolytic ATP production were dissociated: while palmitate-induced mitochondrial fragmentation required the presence of both glutamine

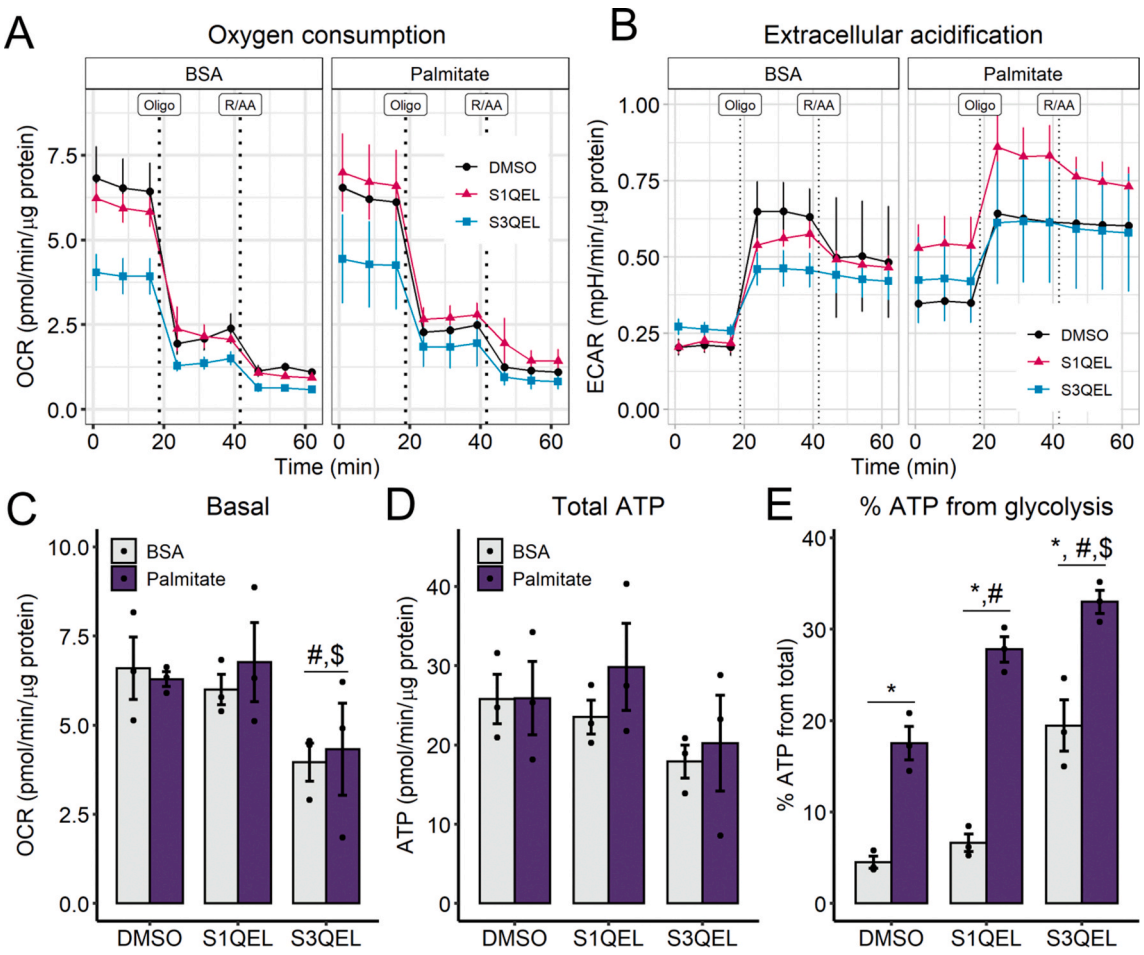

Fig. 8. Inhibition of hydrogen peroxide/superoxide production at site I_Q increases palmitate-induced glycolytic ATP rates - Cells were incubated concomitantly with 10 μM S1QEL or S3QEL and palmitate/BSA (0.2 mM/0.25%) for 6 h. Vehicle is 0.1% DMSO. Real-time OCRs and ECARs were measured in a Seahorse XFe24 analyzer. ATP production was calculated as described in the Methods section. * = $p < 0.05$ vs BSA, # = $p < 0.05$ vs DMSO, $ = vs S1QEL. Two-way ANOVA and Tukey's post-test. Line plots are mean +/- SEM. Bar plots are means +/- SD. Filled circles represent independent experiments. (n = 3).

and glucose, palmitate-induced increases in ATP production from glycolysis required only glucose (Fig. 4). Glutamine starvation was described recently as a strong pro-fusion signal [51], so we speculate that glutamine and/or glucose starvation are hierarchically stronger signals that favor elongation [52] compared to palmitate-induced fragmentation. Carbon flux through glycerol-3-phosphate consumption may contribute toward the morphology-independent palmitate-induced increase in glycolytic flux we observed. Indeed, glycerolipid synthesis has been recently shown to be increased by palmitate, resulting in diacylglycerol accumulation [9], and is expected to involve enhanced glycolytic flux in hepatic cells.

Another clear metabolic effect of palmitate was an increase in total NAD(P)H, and a shift to a more oxidized redox state of the pyridine nucleotide pool. Together, these suggest chronic oxidative imbalance, depleting NAD(P)H and increasing compensatory pyridine nucleotide synthesis. Palmitate was shown to activate production of superoxide by NADPH oxidases in many cell types, including skeletal muscle, pancreatic islets, endothelial cells, and hepatocytes [53,54,55,56]. Furthermore, the ability of palmitate to both decrease nicotinamide nucleotide transhydrogenase (NNT) [57] content and inhibit it [58] make this enzyme a notable redox control node, integrating redox state and substrate use during lipotoxicity in mitochondria. Indeed, NNT is seminal in the control of NADPH content in the mitochondrial matrix, responsible for the maintenance of ~50% of the NADPH pool [33]. Since the discovery of a spontaneous NNT mutation in Jax C57BL/6 J mice [59], NNT importance has been increasingly recognized, as mice lacking the functional enzyme are more sensitive to diet-induced metabolic diseases [60–62].

Based on the significant change in NAD(P)H/$NAD(P)^+$ ratios (Fig. 5A), we hypothesized that the activation of glycolysis could be the result of redox regulation. Indeed, we found that oxidant-generating menadione increased glycolytic flux without disturbing total ATP production nor mitochondrial ATP-linked respiration (Fig. 6). On the other hand, the antioxidant MitoQ severely impacted upon mitochondrial function when at concentrations higher than 0.5 μM (Fig. 7), a finding which indicates that effects of MitoQ in the literature that are not accompanied by respiratory measurements as controls may not be specifically attributable to its antioxidant effects. Notably, the glycolytic shift promoted by palmitate plus 0.5 μM MitoQ was higher than under control conditions, suggesting that the production of mitochondrial oxidants may play a synergistic role in the induction of glycolysis by palmitate. It has not escaped our attention that this redox-regulatory role is not linear, and that both menadione, an oxidant, and MitoQ, an antioxidant, result in glycolytic activation. However, both redox and metabolic regulation are complex, and thus would not be expected to act as simple antagonistic switches.

Recently, Brand's group generated tools to investigate the role of reactive oxygen species production by the electron transport chain in cell biology [38,39]. They found small molecules (S1QEL and S3QEL) that block, specifically, the production of superoxide/hydrogen peroxide at complexes I and III, respectively, without disturbing electron flow to oxygen, nor the production of oxidants at other sites. We took

advantage of these molecules and identified that palmitate-induced glycolysis is exacerbated by the inhibition of superoxide/hydrogen peroxide at site I_Q (Fig. 8), a location within mitochondrial complex I that produces both superoxide and hydrogen peroxide, toward the matrix. Site III_Q produces superoxide toward both the matrix and the intermembrane space. Curiously, S3QEL increased glycolysis in both BSA and palmitate groups. However, since OCRs were significantly inhibited by it, we cannot exclude that other effects may be associated with this increase. This respiratory inhibition was not observed with S1QEL, which nonetheless affected glycolytic ATP production (Fig. 8). Based on the abundant results of the set of mitochondrial antioxidants tested, we conclude that the production of oxidants, and particularly the I_Q site production site, is associated with metabolic rewiring of glycolysis promoted by palmitate, leading to lipotoxicity.

4. Conclusions

Our work uncovers significant early metabolic effects promoted by palmitate lipotoxicity in hepatic cells. We found that palmitate relies on glutamine and glucose availability to promote mitochondrial fragmentation. However, mitochondrial ATP production is unperturbed by a high degree of mitochondrial network fragmentation and oxidative imbalance, while glycolysis is readily responsive to acute palmitate treatment, oxidative imbalance, and mitochondrial oxidant production. Interestingly, inhibition of superoxide/hydrogen peroxide production at complex I site I_Q was sensitive to palmitate and activated glycolysis. This indicates a novel, fatty acid-modulated redox regulation of glycolytic ATP production.

5. Methods

5.1. Cell cultures, palmitate conjugation and lipotoxic incubation

Human hepatoma PLC/PRF/5 cells, or "Alexander cells", were maintained in Dulbecco's Modified Eagle Medium (DMEM) containing 5.5 mM glucose, 4 mM glutamine, 1 mM pyruvate, 25 mM Hepes, 1% penicillin/streptomycin, and 10% fetal bovine serum, in a humidified, 5% CO_2, 37 °C incubator.

Sodium palmitate was solubilized in MilliQ water by heating (70 °C) and conjugated to fatty acid-free bovine serum albumin (which we will refer to as BSA in the rest of the methods section) at 37 °C. A stock solution (4 mM fatty acid in 5% albumin) was filtered (0.22 μm) and frozen under sterile conditions at −20 °C for later use.

Prior to experiments, cells were plated in maintenance DMEM for 24 h, and then PBS-washed and the medium was replaced by DMEM in the presence or absence of 5.5 mM glucose and 4 mM glutamine, supplemented with sodium palmitate conjugated to BSA to final a concentration of 200 μM in 0.25% BSA. Control groups were incubated in 0.25% FFA BSA.

5.2. SDS PAGE and western blots

After incubation with fatty acids, cells were lysed in RIPA buffer and centrifuged (16,000 g, 30 min). The supernatant was collected, and protein quantification was performed using Pierce's BCA reagent and a BSA standard curve. Proteins were diluted in Laemli buffer containing 5% β-mercaptoethanol and heated for 5 min for denaturation. Proteins were separated by electrophoresis in a denaturing polyacrylamide gel and transferred to a polyvinylidene difluoride (PVDF) membrane. After blocking with 5% defatted milk, membranes were incubated (overnight, 4 °C) with primary antibodies. Membranes were then incubated with secondary antibodies conjugated to fluorescent (Licor®) anti-mouse or anti-rabbit.

5.3. Confocal microscopy and image analysis

Mitotracker Deep Red (50 nM, ThermoScientific®), or methyl tetramethylrhodamine ester (TMRM 100 nM, ThermoScientific®) and BODIPY 493/503 (0.2 μg mL^{-1}, ThermoScientific®) were added to the cells (plated on 4-chamber CELLView, Greiner BioOne®) for 30 min at 37 °C and 5% CO_2. Immediately after, live cell images were acquired using a Zeiss LSM 880 Elyra Ayriscan confocal microscope (temperature, humidity and CO_2 control). The acquisition was made at 35 positions on the Z axis, in order to enable reconstruction in 3 dimensions, or 7 positions on the Z axis and 9 XY blocks, in order to quantify the population.

The mitochondrial network was reconstructed in 3D with the aid of MitoKondrY macro for ImageJ, developed by Dr. Sebastien Tosi (IRB Barcelona). Briefly, the macro allows quantification in pixels of the volume and the length of the mitochondrial network. From that, objects that do not form branches (not contained in the network) are identified, filtered as "individuals" for further quantification of their volume, surface area, axis length, sphericity, and aspect ratio (major axis/minor axis). Mitochondrial population evaluation took place after blind identification and sample randomization. Previous definitions were followed: predominantly fragmented - classified as "short" - or predominantly elongated - called "long". The cells called "intermediate" present a network with some proportion of both the shortened and elongated phenotypes. Cells were classified and counted for later identification (Muñoz and Zorzano, 2015). The mitochondrial fusion factor (FF) is defined as % intermediate cells + 2*% elongated cells [24].

5.4. Lactate production

Twenty-four hours after cells plating on P24 plates, cells were incubated with palmitate or BSA as described above. Media were collected at 0, 1, 3, and 6 h, and the cells were PBS-washed and frozen. Secreted lactate was measured in the media using a colorimetric assay, following the manufacturer's instructions (LabTest®, Brazil). Values were normalized by total cell protein content.

5.5. Triglyceride content

After cell incubation on 10 cm plates, cells were PBS-washed and scraped in 1 mL PBS. Eight hundred microliters were centrifuged and 200 μL were kept for protein quantification. After centrifugation (5 min, 300 g), lipids were extracted by Folch's method (adapted from Folch et al. [63]; Wang et al. [64]). Briefly, the pellets were resuspended in 1 mL chloroform:methanol (2:1) and vigorously agitated for 1 h. Two-hundred microliters of MilliQ water were added to the tube and vortexed. The organic phase was collected to a new tube and dried overnight in the fume hood. The pellet was resuspended in 200 μL chloroform and 2% Triton-X 100 and re-dried. The remaining pellet was resuspended in 50 μL MilliQ water and the triglyceride content was measured by a colorimetric assay, following the manufacturer's instructions (LabTest®, Brazil). Values were normalized to the total cell protein content.

5.6. Metabolic analysis: oxygen consumption, extracellular acidification rates, and ATP production

5.6.1. Palmitate overload: permeabilized cell oxygen consumption

Mitochondrial respiration in permeabilized PLC cells was assessed using a high-resolution Oroboros Oxygraph. After 6 h in 200 μM/0.25% palmitate/BSA or 0.25% BSA, cells on 10 cm dishes were PBS-washed and tripsinized. Half a million cells were suspended in 2 mL of experimental buffer (125 mM sucrose, 65 mM KCl, 10 mM Hepes, 2 mM phosphate, 2 mM $MgCl_2$, 2 mM EGTA and 0.2% BSA; pH adjusted to 7.2 with KOH) and permeabilized with 0.001% digitonin (the ideal concentration was determined using previous titration assays) [25,26]. Four different combinations of substrates were employed for each trace: 1

mM pyruvate and 1 mM malate; 1 mM glutamate plus 1 mM malate; 1 mM succinate plus 1 μM rotenone; and "all", comprising of 1 mM succinate, 1 mM malate, 1 mM glutamate and 1 mM pyruvate. State 3 and State 4 were induced using 10 mM ADP and 1.3 μM oligomycin, respectively. Respiratory control ratios were determined as State 3/State 4.

5.6.2. Palmitate overload: real-time intact cell oxygen consumption and extracellular acidification rates

Twenty-four hours after plating on XFe24 Seahorse plates (Agilent®), cells were PBS-washed and incubated in DMEM containing 5.5 mM glucose, 4 mM glutamine, 1 mM pyruvate, 1% penicillin/streptomycin, and 5 mM Hepes. Media did not contain bicarbonate nor FBS. Cells were kept for 30 min in a humidified 37 °C incubator. After basal oxygen consumption and extracellular acidification rates (OCR and ECAR, respectively) were measured, sodium palmitate conjugated to fatty acid free BSA was injected into the wells to final concentrations of 200 μM/0.25%. Control groups received 0.25% fatty acid free BSA. Measurements were taken after the injection and at every hour, up to 6 h. Cell-free wells were incubated with BSA or palmitate/BSA for background correction, calculated by subtracting changes observed from the experiments in the presence of cells.

5.6.3. Palmitate overload: glycolysis modulation with 2-deoxyglucose

Twenty-four hours after plating on XFe24 Seahorse plates (Agilent®), cells were PBS-washed and incubated in DMEM containing 5.5 mM glucose, 4 mM glutamine, 1 mM pyruvate, 1% penicillin/streptomycin, 200 μM/0.25% palmitate/BSA, 5 mM Hepes. Control groups received 0.25% BSA. Media did not contain bicarbonate nor FBS. Cells were kept for 6 h in a humidified 37 °C incubator. OCR and ECAR were measured under basal conditions and following the addition of 20 mM 2-deoxyglucose, 1 μM oligomycin (pre-titrated), 1 μM rotenone and 1 μM antimycin A. ATP production rates (glycolytic, mitochondrial, and total) were calculated from the ECAR, OCR, and proton exchange rate ($PER = ECAR*BF*Vol_{microchamber}*K_{vol}$), following the manufacturer's instructions. Briefly, mitochondrial-derived ATP is $(OCR_{basal} - OCR_{oligomycin})*P/O$. Glycolytic ATP is $PER_{Total} - (OCR_{basal} - OCR_{Rot/AA})*CCF$. Total ATP production is the sum of mitochondrial and glycolytic ATP. We used the manufacturer's standard values for K_{vol}, P/O (phosphate/oxygen ratio) and CCF (CO_2 contribution factor). BF (buffer factor) was previously measured as 3.13 $mM \cdot pH^{-1}$.

5.6.4. Palmitate overload: glucose and/or glutamine deprivation

Twenty-four hours after plating on XFe24 Seahorse plates (Agilent®), cells were PBS-washed and incubated in DMEM containing 1 mM pyruvate, 1% penicillin/streptomycin, 200 μM/0.25% palmitate/BSA, and 5 mM Hepes. Eight groups were assigned for nutrient deprivation experiments (with or without palmitate): i) N/A: without glucose and glutamine, ii) Glc + Gln: added glucose and glutamine, iii) Glc: added glucose, iv) added glutamine. Concentrations for glucose and glutamine were 5.5 mM and 4 mM, respectively. Control groups received 0.25% BSA. Media did not contain bicarbonate nor FBS. Cells were kept for 6 h in a humidified 37 °C incubator. Oxygen consumption and extracellular acidification rates were measured under basal conditions, and with 1 μM oligomycin followed by 1 μM rotenone and 1 μM antimycin A. ATP production rates were calculated as described in the manufacturer's instructions. The buffer factors were previously measured for each buffer (in $mM \cdot pH^{-1}$): Glc + Gln = 3.13, Glc = 3.34, Gln = 3.13, No-additions = 3.6.

5.6.5. Palmitate overload: oxidant production modulation

Twenty-four hours after plating on XFe24 Seahorse plates (Agilent®), cells were PBS-washed and incubated in DMEM containing 5.5 mM glucose, 4 mM glutamine, 1 mM pyruvate, 1% penicillin/streptomycin, 200 μM/0.25% palmitate/BSA, 5 mM Hepes, and 10 μM atglistatin, S1QEL 1.1, S3QEL 2, or menadione. Control groups received 0.25% BSA and/or 0.1% DMSO as vehicle. Media did not contain bicarbonate nor FBS. Cells were kept for 6 h in a humidified 37 °C incubator. Oxygen consumption and extracellular acidification rates were measured under basal conditions, and after the addition of 1 μM oligomycin followed by 1 μM rotenone and 1 μM antimycin A. ATP production rates were calculated as described in the manufacturer's instructions.

For MitoQ titration, after washing with PBS and changing to media without bicarbonate, cells were kept for 30 min in a humidified 37 °C incubator. After basal oxygen consumption and extracellular acidification rates were measured, MitoQ was injected into the wells to a final concentration of 0.1, 0.5, and 1.0 μM. OCR and ECAR were immediately acquired, following sodium palmitate conjugated to BSA injection to a final concentration of 200 μM/0.25%. Control groups received 0.25% BSA. Every hour, measurements were taken up to 2 h, following the addition of 1 μM oligomycin (pre-titrated), 1 μM rotenone and 1 μM antimycin A. ATP production rates (glycolytic, mitochondrial, and total) were calculated from the ECAR, OCR, and PER considering the rates at 2 h.

5.6.6. Protein normalization

After every run, the media was removed, and the cells were frozen. Post-thawing, cells were disrupted by RIPA buffer and vigorous agitation. Protein quantification was performed using Pierce's BCA reagent and a BSA standard curve.

5.7. NAD(P)H

After 6 h in 200 μM/0.25% palmitate/BSA or 0.25% BSA, cells plated on 10 cm dishes were PBS-washed and tripsinized. Cells were resuspended in DMEM with 5.5 mM glucose, 4 mM glutamine, 1 mM pyruvate and 5 mM Hepes, and counted. Half a million cells per milliliter were incubated in DMEM containing 200 μM/0.25% palmitate. NAD(P)H fluorescence (excitation 366 nm, emission 450 nm) was followed in a F4500 Hitachi® fluorimeter with magnetic stirring. Cells were challenged with two sequential additions of *t*-butyl hydroperoxide (0.5 mM) every 5 min. After 3 min, oligomycin (1 μM), carbonyl cyanide 3-chlorophenylhydrazone (CCCP, 1 μM – to promote maximal oxidation), and rotenone (1 μM) plus antimycin A (1 μM), to promote maximal reduction, were sequentially added.

5.8. Hydrogen peroxide production

Mitochondrial hydrogen peroxide release was followed in permeabilized cells through the oxidation of Amplex Red catalyzed by horseradish peroxidase [45]. After 6 h in 200 μM/0.25% palmitate/BSA or 0.25% BSA, cells plated on 10 cm dishes were PBS-washed and tripsinized. Half a million cells were suspended in 2 mL of experimental buffer (125 mM sucrose, 65 mM KCl, 10 mM Hepes, 2 mM phosphate, 2 mM $MgCl_2$, 2 mM EGTA and 0.2% BSA; pH was adjusted with KOH at 7.2 units) and permeabilized with 0.001% digitonin, a concentration determined in preliminary experiments to selectively permeabilize the plasma membrane [25,26]. The oxidation of Amplex Red generates the fluorescent compound resorufin and its formation was followed with a F4500 Hitachi Fluorimeter at excitation and emission wavelength of 563 nm and 587 nm, respectively, at 37 °C and constant stirring. Two different combinations of substrates were employed: 1 mM succinate, 1 mM malate, 1 mM glutamate and 1 mM pyruvate (named "all" in the figure); and 1 mM succinate. In each trace, peroxide release was modulated by the sequential addition of 1 mM ADP (State 3), 1.3 μM oligomycin (State 4), and 1 μM rotenone or 10 μM S1QEL. Calibration used a hydrogen peroxide standard curve.

5.9. Statistics

The analyses were conducted using Microsoft Excel, RStudio, or

JASP. Outliers were removed by Grubb's test (alpha = 0.05). Group means were compared by Student's *t*-test or Analysis of Variance (ANOVA) followed by Tukey's post-test, according to the experimental design. Levels of significance were considered at $p < 0.05$.

6. Materials

Culture media, supplements, TMRM, MitoTracker Deep Red, BODIPY 493/503, and Amplex Red were purchased from Thermo Scientific, except for DMEM with no glucose (cat. D5030), from Sigma Aldrich. Oligomycin, rotenone, and antimycin A were from Santa Cruz Biotechnology. Mitoquinone is from Medkoo Biosciences. The primary antibodies are from Cell Signaling (anti-MFN1 cat. 14739 S, anti-MFN2 cat. 9482 S, anti-DRP1 cat. 3455 S) or Abcam (β-actin cat. ab8226). The secondary antibodies are from Licor. Triglyceride's kit was from LabTest. All the other reagents were purchased from Sigma-Aldrich.

7. Data availability

All data presented and discussed are contained within the article or the supporting material.

Declaration of competing interest

The authors have no conflict of interests to declare.

Acknowledgments

The authors thank Camille Caldeira da Silva, Dr. Juan Pablo Muñoz, Dr. María Isabel Hernández-Alvarez, Jordi Seco, Dr. Sebastien Tosi, and Dr. Nikolaos Giakoumakis for excellent technical support and experimental help, and Dr. Bruno Chausse for manuscript revision.

Appendix A. Supplementary data

Supplementary data to this article can be found online at https://doi.org/10.1016/j.redox.2021.102026.

Author contributions

Conceived and designed the experiments: PK, AZ and AK. Performed the experiments: PK, JDS, and VR. Analyzed the data: PK, JDS, and VR. Contributed reagents/materials/analysis tools: AZ, AK. Wrote the manuscript: PK and AK. Reviewed final version of the manuscript: PK, JDS, VR, AZ and AK.

Funding

This work was funded by *Centro de Pesquisa, Inovação e Difusão de Processos Redox em Biomedicina* (CEPID Redoxoma) grant 2013/07937–8, *Fundação de Amparo à Pesquisa do Estado de São Paulo* (FAPESP) grants 2015/25862-0, 2019/05226-3, 2019/18402-4, MINECO (SAF2016-75246R), the Generalitat de Catalunya (Grant 2017SGR1015), CIBERDEM ("Instituto de Salud Carlos III"), the Fundación Ramon Areces (CIVP18A3942), the Fundación BBVA, Fundació Marató de TV3 (20132330), and CAPES, with no involvement of the funding agencies in the design of this study.

References

[1] A. Tchernof, J.-P. Després, Pathophysiology of human visceral obesity: an update, Physiol. Rev. 93 (2013) 359–404, https://doi.org/10.1152/physrev.00033.2011.
[2] T. Hardy, F. Oakley, Q.M. Anstee, C.P. Day, Nonalcoholic fatty liver disease: pathogenesis and disease spectrum, Annu. Rev. Pathol. 11 (2016) 451–496, https://doi.org/10.1146/annurev-pathol-012615-044224.
[3] R. Feng, C. Luo, C. Li, S. Du, A.P. Okekunle, Y. Li, et al., Free fatty acids profile among lean, overweight and obese non-alcoholic fatty liver disease patients: a case – control study, Lipids Health Dis. 16 (2017) 165, https://doi.org/10.1186/s12944-017-0551-1.
[4] O. Quehenberger, A.M. Armando, A.H. Brown, S.B. Milne, D.S. Myers, A.H. Merrill, et al., Lipidomics reveals a remarkable diversity of lipids in human plasma, J. Lipid Res. 51 (2010) 3299–3305, https://doi.org/10.1194/jlr.M009449.
[5] K. Tomita, T. Teratani, H. Yokoyama, T. Suzuki, R. Irie, H. Ebinuma, et al., Plasma free myristic acid proportion is a predictor of nonalcoholic steatohepatitis, Dig. Dis. Sci. 56 (2011) 3045–3052, https://doi.org/10.1007/s10620-011-1712-0.
[6] M.E. Ertunc, G.S. Hotamisligil, Lipid signaling and lipotoxicity in metaflammation: indications for metabolic disease pathogenesis and treatment, J. Lipid Res. 57 (2016) 2099–2114, https://doi.org/10.1194/jlr.R066514.
[7] N. Alsabeeh, B. Chausse, P.A. Kakimoto, A.J. Kowaltowski, O. Shirihai, Cell culture models of fatty acid overload: problems and solutions, Biochim. Biophys. Acta BBA - Mol. Cell Biol. Lipids 1863 (2018) 143–151, https://doi.org/10.1016/j.bbalip.2017.11.006.
[8] L.D. Ly, S. Xu, S.-K. Choi, C.-M. Ha, T. Thoudam, S.-K. Cha, et al., Oxidative stress and calcium dysregulation by palmitate in type 2 diabetes, Exp. Mol. Med. 49 (2018) e291, https://doi.org/10.1038/emm.2016.157.
[9] M. Piccolis, L.M. Bond, M. Kampmann, P. Pulimeno, C. Chitraju, C.B.K. Jayson, et al., Probing the global cellular responses to lipotoxicity caused by saturated fatty acids, Mol. Cell 74 (2019) 32–44, https://doi.org/10.1016/j.molcel.2019.01.036, e8.
[10] M. Masuda, S. Miyazaki-Anzai, A.L. Keenan, K. Okamura, J. Kendrick, M. Chonchol, et al., Saturated phosphatidic acids mediate saturated fatty acid–induced vascular calcification and lipotoxicity, J. Clin. Invest. 125 (2015) 4544–4558, https://doi.org/10.1172/JCI82871.
[11] X.G. Zhu, S. Nicholson Puthenveedu, Y. Shen, K. La, C. Ozlu, T. Wang, et al., CHP1 regulates compartmentalized glycerolipid synthesis by activating GPAT4, Mol. Cell 74 (2019) 45–58, https://doi.org/10.1016/j.molcel.2019.01.037, e7.
[12] D. Sebastián, M. Palacín, A. Zorzano, Mitochondrial dynamics: coupling mitochondrial fitness with healthy aging, Trends Mol. Med. 23 (2017) 201–215, https://doi.org/10.1016/j.molmed.2017.01.003.
[13] D.C. Chan, Mitochondrial dynamics and its involvement in disease, Annu. Rev. Pathol. 15 (2020) 235–259, https://doi.org/10.1146/annurev-pathmechdis-012419-032711.
[14] Z. Cheng, Y. Tseng, M.F. White, Insulin signaling meets mitochondria in metabolism, Trends Endocrinol. Metabol. 21 (2010) 589–598, https://doi.org/10.1016/j.tem.2010.06.005.
[15] A. del Campo, V. Parra, C. Vásquez-Trincado, T. Gutiérrez, P.E. Morales, C. López-Crisosto, et al., Mitochondrial fragmentation impairs insulin-dependent glucose uptake by modulating Akt activity through mitochondrial Ca2+ uptake, AJP Endocrinol. Metab. 306 (2014) E1–E13, https://doi.org/10.1152/ajpendo.00146.2013.
[16] A. Zorzano, M.I. Hernández-Alvarez, D. Sebastián, J.P. Muñoz, Mitofusin 2 as a driver that controls energy metabolism and insulin signaling, Antioxidants Redox Signal. 22 (2015) 1020–1031, https://doi.org/10.1089/ars.2014.6208.
[17] T. Wai, T. Langer, Mitochondrial dynamics and metabolic regulation, Trends Endocrinol. Metabol. 27 (2016) 105–117, https://doi.org/10.1016/j.tem.2015.12.001.
[18] I. Gordaliza-Alaguero, C. Cantó, A. Zorzano, Metabolic implications of organelle–mitochondria communication, EMBO Rep. (2019), e47928, https://doi.org/10.15252/embr.201947928, 0.
[19] M. Liesa, O.S. Shirihai, Mitochondrial dynamics in the regulation of nutrient utilization and energy expenditure, Cell Metabol. 17 (2013) 491–506, https://doi.org/10.1016/j.cmet.2013.03.002.
[20] E. Schrepfer, L. Scorrano, Mitofusins, from mitochondria to metabolism, Mol. Cell 61 (2016) 683–694, https://doi.org/10.1016/j.molcel.2016.02.022.
[21] A.J.A. Molina, J.D. Wikstrom, L. Stiles, G. Las, H. Mohamed, A. Elorza, et al., Mitochondrial networking protects β-cells from nutrient-induced apoptosis, Diabetes 58 (2009) 2303–2315, https://doi.org/10.2337/db07-1781.
[22] H.-F. Jheng, P.-J. Tsai, S.-M. Guo, L.-H. Kuo, C.-S. Chang, I.-J. Su, et al., Mitochondrial fission contributes to mitochondrial dysfunction and insulin resistance in skeletal muscle, Mol. Cell Biol. 32 (2012) 309–319, https://doi.org/10.1128/MCB.05603-11.
[23] S.S. Kulkarni, M. Joffraud, M. Boutant, J. Ratajczak, A.W. Gao, C. Maclachlan, et al., Mfn1 deficiency in the liver protects against diet-induced insulin resistance and enhances the hypoglycemic effect of metformin, Diabetes (2016) 1–40.
[24] D. Senyilmaz, S. Virtue, X. Xu, C.Y. Tan, J.L. Griffin, A.K. Miller, et al., Regulation of mitochondrial morphology and function by stearoylation of TFR1, Nature 525 (2015) 124–128, https://doi.org/10.1038/nature14601.
[25] G. Fiskum, S.W. Craig, G.L. Decker, A.L. Lehninger, The cytoskeleton of digitonin-treated rat hepatocytes, Proc. Natl. Acad. Sci. Unit. States Am. 77 (1980) 3430–3434, https://doi.org/10.1073/pnas.77.6.3430.
[26] A.J. Kowaltowski, S.L. Menezes-Filho, E.A. Assali, I.G. Gonçalves, J.V. Cabral-Costa, P. Abreu, et al., Mitochondrial morphology regulates organellar Ca2+ uptake and changes cellular Ca2+ homeostasis, FASEB J., fj.201901136R (2019), https://doi.org/10.1096/fj.201901136R.
[27] S.A. Mookerjee, R.L.S. Goncalves, A.A. Gerencser, D.G. Nicholls, M.D. Brand, The contributions of respiration and glycolysis to extracellular acid production, Biochim. Biophys. Acta BBA - Bioenerg. 1847 (2015) 171–181, https://doi.org/10.1016/j.bbabio.2014.10.005.
[28] K.T. Ong, M.T. Mashek, S.Y. Bu, A.S. Greenberg, D.G. Mashek, Adipose triglyceride lipase is a major hepatic lipase that regulates triacylglycerol turnover and fatty acid signaling and partitioning, Hepatology 53 (2011) 116–126, https://doi.org/10.1002/hep.24006.

[29] A. Sathyanarayan, M.T. Mashek, D.G. Mashek, ATGL promotes autophagy/lipophagy via SIRT1 to control hepatic lipid droplet catabolism, Cell Rep. 19 (2017) 1–9, https://doi.org/10.1016/j.celrep.2017.03.026.
[30] C. Desbois-Mouthon, M.-J.B. Eggelpoë, E. Beurel, M. Boissan, R. Delélo, A. Cadoret, et al., Dysregulation of glycogen synthase kinase-3β signaling in hepatocellular carcinoma cells, Hepatology 36 (2002) 1528–1536, https://doi.org/10.1002/hep.1840360630.
[31] A.R. Cardoso, P.A.H.B. Kakimoto, A.J. Kowaltowski, Diet-sensitive sources of reactive oxygen species in liver mitochondria: role of very long chain acyl-CoA dehydrogenases, PloS One 8 (2013), e77088, https://doi.org/10.1371/journal.pone.0077088.
[32] P.A. Kakimoto, A.J. Kowaltowski, Effects of high fat diets on rodent liver bioenergetics and oxidative imbalance, Redox Biol 8 (2016) 216–225, https://doi.org/10.1016/j.redox.2016.01.009.
[33] J. Rydström, Mitochondrial NADPH, transhydrogenase and disease, Biochim. Biophys. Acta BBA - Bioenerg. 1757 (2006) 721–726, https://doi.org/10.1016/j.bbabio.2006.03.010.
[34] C.C. Winterbourn, Biological production, detection, and fate of hydrogen peroxide, Antioxidants Redox Signal. 29 (2018) 541–551, https://doi.org/10.1089/ars.2017.7425.
[35] W. Xiao, J. Loscalzo, Metabolic responses to reductive stress, Antioxidants Redox Signal. (2019), https://doi.org/10.1089/ars.2019.7803.
[36] P.F. Smith, D.W. Alberts, G.F. Rush, Menadione-induced oxidative stress in hepatocytes isolated from fed and fasted rats: the role of NADPH-regenerating pathways, Toxicol. Appl. Pharmacol. 89 (1987) 190–201, https://doi.org/10.1016/0041-008X(87)90040-8.
[37] R.A.J. Smith, M.P. Murphy, Animal and human studies with the mitochondria-targeted antioxidant MitoQ, Ann. N. Y. Acad. Sci. 1201 (2010) 96–103, https://doi.org/10.1111/j.1749-6632.2010.05627.x.
[38] A.L. Orr, L. Vargas, C.N. Turk, J.E. Baaten, J.T. Matzen, V.J. Dardov, et al., Suppressors of superoxide production from mitochondrial complex III, Nat. Chem. Biol. 11 (2015) 834–836, https://doi.org/10.1038/nchembio.1910.
[39] M.D. Brand, R.L.S. Gonçalves, A.L. Orr, L. Vargas, A.A. Gerencser, M. Borch Jensen, et al., Suppressors of superoxide-H2O2 production at site IQ of mitochondrial complex I protect against stem cell hyperplasia and ischemia-reperfusion injury, Cell Metabol. 24 (2016) 582–592, https://doi.org/10.1016/j.cmet.2016.08.012.
[40] B. Chausse, P.A. Kakimoto, C.C. Caldeira-da-Silva, A.B. Chaves-Filho, M. Y. Yoshinaga, R.P. da Silva, et al., Distinct metabolic patterns during microglial remodeling by oleate and palmitate, Biosci. Rep. 39 (2019), https://doi.org/10.1042/BSR20190072.
[41] J. Bao, I. Scott, Z. Lu, L. Pang, C.C. Dimond, D. Gius, et al., SIRT3 is regulated by nutrient excess and modulates hepatic susceptibility to lipotoxicity, Free Radic. Biol. Med. 49 (2010) 1230–1237, https://doi.org/10.1016/j.freeradbiomed.2010.07.009.
[42] R.A. Egnatchik, A.K. Leamy, Y. Noguchi, M. Shiota, J.D. Young, Palmitate-induced activation of mitochondrial metabolism promotes oxidative stress and apoptosis in H4IIEC3 rat hepatocytes, Metabolism 63 (2014) 283–295, https://doi.org/10.1016/j.metabol.2013.10.009.
[43] Y. Geng, A. Hernández Villanueva, A. Oun, M. Buist-Homan, H. Blokzijl, K. N. Faber, et al., Protective effect of metformin against palmitate-induced hepatic cell death, Biochim. Biophys. Acta BBA - Mol. Basis Dis. 1866 (2020) 165621, https://doi.org/10.1016/j.bbadis.2019.165621.
[44] R.A. Egnatchik, A.K. Leamy, D.A. Jacobson, M. Shiota, J.D. Young, ER calcium release promotes mitochondrial dysfunction and hepatic cell lipotoxicity in response to palmitate overload, Mol. Metab. 3 (2014) 544–553, https://doi.org/10.1016/j.molmet.2014.05.004.
[45] M. Zhou, Z. Diwu, N. Panchuk-Voloshina, R.P. Haugland, A stable nonfluorescent derivative of resorufin for the fluorometric determination of trace hydrogen peroxide: applications in detecting the activity of phagocyte NADPH oxidase and other oxidases, Anal. Biochem. 253 (1997) 162–168, https://doi.org/10.1006/abio.1997.2391.
[46] M.D. Brand, D.G. Nicholls, Assessing mitochondrial dysfunction in cells, Biochem. J. 435 (2011) 297–312, https://doi.org/10.1042/BJ20110162.
[47] A.A. Gerencser, C. Chinopoulos, M.J. Birket, M. Jastroch, C. Vitelli, D.G. Nicholls, et al., Quantitative measurement of mitochondrial membrane potential in cultured cells: calcium-induced de- and hyperpolarization of neuronal mitochondria, J. Physiol. 590 (2012) 2845–2871, https://doi.org/10.1113/jphysiol.2012.228387.
[48] A.J. Kowaltowski, R.G. Cosso, C.B. Campos, G. Fiskum, Effect of Bcl-2 overexpression on mitochondrial structure and function, J. Biol. Chem. 277 (2002) 42802–42807, https://doi.org/10.1074/jbc.M207765200.
[49] A.S. Divakaruni, W.Y. Hsieh, L. Minarrieta, T.N. Duong, K.K.O. Kim, B.R. Desousa, et al., Etomoxir inhibits macrophage polarization by disrupting CoA homeostasis, Cell Metabol. 28 (2018) 490–503, https://doi.org/10.1016/j.cmet.2018.06.001, e7.
[50] R.A. Egnatchik, A.K. Leamy, S.A. Sacco, Y.E. Cheah, M. Shiota, J.D. Young, Glutamate–oxaloacetate transaminase activity promotes palmitate lipotoxicity in rat hepatocytes by enhancing anaplerosis and citric acid cycle flux, J. Biol. Chem. 294 (2019) 3081–3090, https://doi.org/10.1074/jbc.RA118.004869.
[51] W.-F. Cai, C. Zhang, Y.-Q. Wu, G. Zhuang, Z. Ye, C.-S. Zhang, et al., Glutaminase GLS1 senses glutamine availability in a non-enzymatic manner triggering mitochondrial fusion, Cell Res. 28 (2018) 865–867, https://doi.org/10.1038/s41422-018-0057-z.
[52] L.C. Gomes, G. Di Benedetto, L. Scorrano, Essential amino acids and glutamine regulate induction of mitochondrial elongation during autophagy, Cell Cycle 10 (2011) 2635–2639, https://doi.org/10.4161/cc.10.16.17002.
[53] D. Morgan, H.R. Oliveira-Emilio, D. Keane, A.E. Hirata, M. Santos da Rocha, S. Bordin, et al., Glucose, palmitate and pro-inflammatory cytokines modulate production and activity of a phagocyte-like NADPH oxidase in rat pancreatic islets and a clonal beta cell line, Diabetologia 50 (2007) 359–369, https://doi.org/10.1007/s00125-006-0462-6.
[54] R.H. Lambertucci, S.M. Hirabara, L. Silveira, R. dos, A.C. Levada-Pires, R. Curi, T. C. Pithon-Curi, Palmitate increases superoxide production through mitochondrial electron transport chain and NADPH oxidase activity in skeletal muscle cells, J. Cell. Physiol. 216 (2008) 796–804, https://doi.org/10.1002/jcp.21463.
[55] Maloney Ezekiel, R. Sweet Ian, M. Hockenbery David, Matilda Pham, O. Rizzo Norma, Tateya Sanshiro, et al., Activation of NF-κB by palmitate in endothelial cells, Arterioscler. Thromb. Vasc. Biol. 29 (2009) 1370–1375, https://doi.org/10.1161/ATVBAHA.109.188813.
[56] A. Bettaieb, J.X. Jiang, Y. Sasaki, T.-I. Chao, Z. Kiss, X. Chen, et al., Hepatocyte nicotinamide adenine dinucleotide phosphate reduced oxidase 4 regulates stress signaling, fibrosis, and insulin sensitivity during development of steatohepatitis in mice, Gastroenterology 149 (2015) 468–480, https://doi.org/10.1053/j.gastro.2015.04.009, e10.
[57] G. McCambridge, M. Agrawal, A. Keady, P.A. Kern, H. Hasturk, B.S. Nikolajczyk, et al., Saturated fatty acid activates T cell inflammation through a nicotinamide nucleotide transhydrogenase (NNT)-dependent mechanism, Biomolecules 9 (2019) 79, https://doi.org/10.3390/biom9020079.
[58] J. Rydström, A.V. Panov, G. Paradies, L. Ernster, Inhibition of mitochondrial nicotinamide nucleotide transhydrogenase by CoA-thioesters of long-chain fatty acids, Biochem. Biophys. Res. Commun. 45 (1971) 1389–1397, https://doi.org/10.1016/0006-291X(71)90175-6.
[59] A.A. Toye, J.D. Lippiat, P. Proks, K. Shimomura, L. Bentley, A. Hugill, et al., A genetic and physiological study of impaired glucose homeostasis control in C57BL/6J mice, Diabetologia 48 (2005) 675–686, https://doi.org/10.1007/s00125-005-1680-z.
[60] K.H. Fisher-Wellman, T.E. Ryan, C.D. Smith, L.A.A. Gilliam, C.-T. Lin, L.R. Reese, et al., A direct comparison of metabolic responses to high-fat diet in C57BL/6J and C57BL/6NJ mice, Diabetes 65 (2016) 3249–3261, https://doi.org/10.2337/db16-0291.
[61] C.D.C. Navarro, T.R. Figueira, A. Francisco, G.A. Dal'Bó, J.A. Ronchi, J.C. Rovani, et al., Redox imbalance due to the loss of mitochondrial NAD(P)-transhydrogenase markedly aggravates high fat diet-induced fatty liver disease in mice, Free Radic. Biol. Med. 113 (2017) 190–202, https://doi.org/10.1016/j.freeradbiomed.2017.09.026.
[62] A. Francisco, J.A. Ronchi, C.D.C. Navarro, T.R. Figueira, R.F. Castilho, Nicotinamide nucleotide transhydrogenase is required for brain mitochondrial redox balance under hampered energy substrate metabolism and high-fat diet, J. Neurochem. 147 (2018) 663–677, https://doi.org/10.1111/jnc.14602.
[63] J. Folch, M. Lees, G.H.S. Stanley, A simple method for the isolation and purification of total lipides from animal tissues, J. Biol. Chem. 226 (1957) 497–509.
[64] L. Wang, J. Zhou, S. Yan, G. Lei, C.-H. Lee, X.-M. Yin, Ethanol-triggered lipophagy requires SQSTM1 in AML12 hepatic cells, Sci. Rep. 7 (2017) 12307.